Time-Split Finite-Volume Method for Three-Dimensional Blunt-Body Flow

ARTHUR W. RIZZI* AND MAMORU INOUYE†
NASA Ames Research Center, Moffett Field, Calif.

An efficient numerical method for calculating plane, axisymmetric, and fully three-dimensional blunt-body flow is presented. It is a second-order-accurate, time-dependent finite-volume procedure that solves the Euler equations in integral conservation-law form. These equations are written with respect to a Cartesian coordinate system in which an embedded mesh adjusts in time to the motion of the bow shock that is automatically captured as part of the weak solution. With such an adjusting mesh, oscillations in flow properties near the shock are shown to be virtually eliminated. The scheme uses a time-splitting concept that accelerates the convergence appreciably. Comparisons are made between computed and experimental results.

Introduction

THE computation of the inviscid subsonic-transonic flowfield about a blunt body has been the focus of numerous numerical investigations during the past 10 to 15 years. Determining the fluid properties of either real or perfect gases about the noses of supersonic and hypersonic airplanes and re-entry spacecraft provides the necessary data for the subsequent evaluation of the radiative and convective heat-transfer rates and boundary-layer effects on the aircraft body. It also serves to initiate the downstream calculation of the supersonic portion of the flowfield about such vehicles.[1-5] Another application for these calculations is the study of transonic flow about blunt leading edges. The need and importance of determining all such flowfields have continued the interest in blunt-body methods, particularly those that will handle complicated three-dimensional geometries at high incidence angles.

At the present time, three general classes of numerical methods are appropriate for the blunt-body problem:[6] 1) inverse method,[7-9] 2) method of integral relations,[10-12] and 3) time-dependent finite-difference methods.[13-32] The latter methods provide a means of treating the problem of inviscid supersonic flow past a blunt body as an initial-value problem since the equations for unsteady flow are always hyperbolic.‡ Results for steady flow are obtained as the limiting state reached asymptotically in time by an unsteady flow with constant freestream conditions, a solid stationary body boundary, and suitably chosen initial conditions. This approach appears to be the most convenient for computing flow with either large asymmetry or extensive transonic regions as well as embedded discontinuities.[14,15] For such cases this numerical technique has two important advantages: being equally suited for computing either subsonic or supersonic flow and being capable of approximating weak solutions of the Euler gasdynamic equations.

The time-dependent methods that have been developed for inviscid compressible flow past blunt bodies traveling at supersonic speeds may be classified according to their order of accuracy in terms of mesh spacing. Evans and Harlow[16,17] introduced the particle-in-cell routine of first-order accuracy which is formulated in a mixed Eulerian-Lagrangian frame of reference and treats the bow shock wave as a continuous compression with steep gradients smeared over several mesh spacings by artificial dissipative terms added to the equations of motion. Eulerian methods that handle the bow shock in a similar manner have been developed by Bohachevsky,[14,18] Gentry et al.,[19] Barnwell,[20] and others. In another approach to this problem, Godunov et al.[21] devised a technique of first order that considers the bow shock as a sharp discontinuity forming the outer boundary of the flow. Masson et al.,[22] McNamara,[23] and Rusanov[24] have extended and used this method to calculate complex flowfields. A computational scheme of second-order accuracy that treats shock waves as finite regions of steep but continuous gradients by means of an effective artificial viscosity introduced as a step width was presented by Lax and Wendroff[25,26] and has been applied by Burstein[27] and others to solve the blunt-body problem. Taking the alternative approach of handling the bow shock as a discontinuous outer boundary, Moretti,[15,28] Barnwell,[29,30] and Li[31] among others have developed second-order procedures using conventional nonsplit differencing schemes. In this paper, an efficient second-order-accurate method is presented for calculating either two- or three-dimensional blunt-body flow by utilizing the time-splitting technique recently introduced by MacCormack and Paullay.[32]

In developing a computational method for flow about practical body shapes, the numerical analyst is faced with a decision—either solve the governing equations in the physical space of the flow and devise special routines for handling the boundary conditions or transform the equations and body shape to a new space where the body is a simple surface on which the boundary conditions can be applied easily. The latter route is the one most frequently taken, probably because most difficulties in treating initial-boundary-value problems are encountered not in solving the differential equations but in attempting to satisfy the boundary conditions. We, however, take the former tack and write the equations of motion in integral conservation-law form, referenced to a Cartesian coordinate system, and solve them in the actual space of the physical flow. By adopting this form of the equations and choosing the body shape to be part of the closed surface surrounding the domain of integration, no coordinate mapping is required; yet easy treatment of boundary points for all practical geometries is still retained. Another advantage is that either simple or very general nonorthogonal, nonequispaced finite-difference grids can be handled with equal facility. Also, use of the strong conservation form§ ensures that

Presented as AIAA Paper 73-133 at the AIAA 11th Aerospace Sciences Meeting, Washington, D.C., January 10–12, 1973; submitted February 20, 1973; revision received June 28, 1973. The authors acknowledge the assistance and guidance that R. W. MacCormack of the Ames Research Center provided in adapting the concepts of his time-splitting numerical method for this application and his continual encouragement throughout the course of this investigation.

Index category: Supersonic and Hypersonic Flow.

* NRC-NASA Postdoctoral Research Associate, presently employed as Research Scientist. Associate Member AIAA.

† Research Scientist. Associate Fellow AIAA.

‡ See Ref. 13 for a recent review of numerical methods for hyperbolic systems of partial differential equations.

§ See Ref. 33 for a discussion of the strong conservation form of the Euler equations.

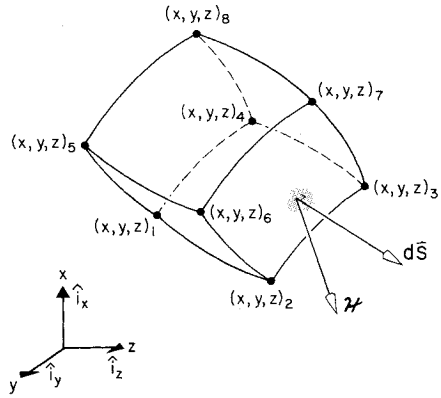

Fig. 1 A general six-sided finite volume of fluid.

solutions containing discontinuities such as shock waves can be accurately computed by considering these discontinuities not as boundaries of the flow but rather as internal features that are acquired automatically by the numerical procedure along with the remaining continuous part of the solution. Adjusting the mesh network so that the outermost cell faces coincide with the shock has been found to virtually eliminate the attendant oscillatory nature of the solution near discontinuities that is so characteristic of these automatic procedures for weak solutions.

Ultimately, the steady state is sought, and maximization of the allowable time step is most advantageous to any numerical method. For this purpose, use of the concept of time splitting reduces a multidimensional, second-order, finite-difference operator appropriate for solving the governing equations to a sequence of essentially one-dimensional operators. This sequence retains the same order of accuracy as that of the unsplit operator, but allows a larger time step to be taken and an overall increase in numerical efficiency to be achieved. These features of the method are demonstrated by comparisons of several blunt-body flowfield computations with experimental measurements as well as with results from other numerical methods.

Theoretical Formulation

The unsteady inviscid equations of fluid dynamics (Euler equations) written in vector integral conservation-law form are

$$\frac{\partial}{\partial t}\iiint_V \mathbf{U}\, d\,\mathrm{vol} + \oiint_S \mathscr{H}\cdot\hat{\eta}\, ds = 0 \qquad (1)$$

where $\mathbf{U}$ is a column vector and $\mathscr{H}$ is a second-order flux tensor whose column elements are three-dimensional flux vectors defined as

$$\mathbf{U} = \begin{bmatrix} \rho \\ \rho u \\ \rho v \\ \rho w \\ e \end{bmatrix} \qquad \mathscr{H}(\mathbf{U}) = \begin{bmatrix} \rho\mathbf{q} \\ \rho u\mathbf{q} + p\hat{i}_x \\ \rho v\mathbf{q} + p\hat{i}_y \\ \rho w\mathbf{q} + p\hat{i}_z \\ (e+p)\mathbf{q} \end{bmatrix}$$

for flow velocity $\mathbf{q}$, total energy e per unit volume, and momentum flux composed of components taken along the unit vector directions $\hat{i}_x$, $\hat{i}_y$, and $\hat{i}_z$ of a rectangular Cartesian coordinate system x, y, z. The velocity referenced to this frame is $\mathbf{q} = u\hat{i}_x + v\hat{i}_y + w\hat{i}_z$. The system is completed by an equation of state $p = p(e, \rho)$ that relates pressure p to internal energy ε and density ρ where $\varepsilon = e/\rho - \frac{1}{2}q^2$. The unit vector $\hat{\eta}$ is the direction of the outer normal to the surface and $\mathscr{H}\cdot\hat{\eta}$ indicates the vector dot product of each column element of $\mathscr{H}$ with $\hat{\eta}$, the result of which is a column vector. This equation, integrated over the surface S enclosing the fluid volume V in a four-dimensional space consisting of three geometric dimensions and time t, expresses the conservation of mass, momentum, and energy within that volume. Using the integral conservation laws directly ensures that shock waves or other gasdynamic discontinuities present in the flow do not interfere with the attainment of the proper solution and can be handled without any special treatment. Referencing the system to Cartesian coordinates guarantees that it will not become indeterminate anywhere in the flowfield and simplifies its form as well as the details of the vector geometry and vector products.

Without any los of generality, the finite volume V of fluid may be specified as a six-sided, boxlike solid with nonplanar faces (a topological hexahedron) homeomorphic to an irregular hexahedron and defined by the eight corner points as drawn in Fig. 1. For such a volume, the closed surface integral over S in Eq. (1) can then be written as

$$\oiint_S \mathscr{H}\cdot\hat{\eta}\, ds = \sum_{l=1}^{6}\iint_{S_l} \mathscr{H}\cdot d\mathbf{s} \qquad (2)$$

where $d\mathbf{s} = \hat{\eta}\, ds$ represents the differential element of surface area for a given side of the hexahedron.

Time-Split Finite-Volume Method

Finite-difference approximations to the gasdynamic conservation laws are used to advance the flow in time from specified initial data. These finite-difference operators will be constructed in this section to solve Eq. (1) for computational cells like the one depicted in Fig. 2. MacCormack and Paullay[32] have shown how these operators can be obtained by splitting a conventional finite-difference method. The resulting operators, essentially one dimensional, are then arranged in sequences so that Eq. (1) is approximated to second-order accuracy.

The numerical domain of dependence of a finite-difference method at a given cell is defined by the surrounding cells from which data are used to advance the solution in time at the given cell by one time step. A necessary condition for most explicit methods is that their numerical domain include the actual physical domain, the Courant-Friedrich-Lewy (CFL) condition, which relates the maximum allowable time-step size to mesh spacing and local flow properties. The ratio of the actual time-step size used in the method to the maximum permitted is termed the CFL number. In our application, we asymptotically march in time to the steady state and naturally want to do everything possible to diminish the computational time required to reach that state. For this purpose, the technique of time splitting can be used to increase computational efficiency by increasing the magnitude of the maximum allowable time step and by reducing the number of needed operations per time cycle.

A two-step difference method of second-order accuracy for numerically solving Eqs. (1) and (2) and directly analogous to those currently being applied to a wide range of problems in fluid dynamics[1-3,15,28-32,34] may be defined as

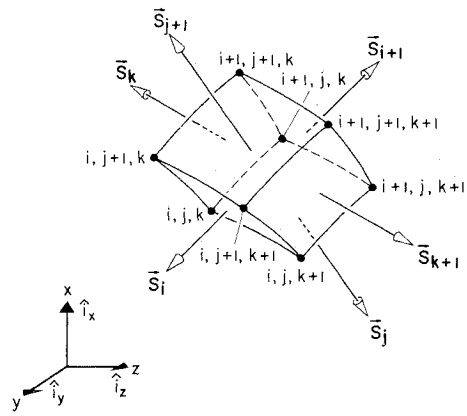

Fig. 2 A typical computational cell i, j, k.

$$\tilde{\mathbf{U}}^{n+1}_{i,j,k} = \mathbf{U}^n_{i,j,k} - \frac{\Delta t}{\mathrm{vol}_{i,j,k}}[\mathscr{H}^n_{i,j,k}\cdot\mathbf{S}_{j+1} + \mathscr{H}^n_{i,j-1,k}\cdot\mathbf{S}_j + \mathscr{H}^n_{i,j,k}\cdot\mathbf{S}_{i+1} + \mathscr{H}^n_{i-1,j,k}\cdot\mathbf{S}_i + \mathscr{H}^n_{i,j,k}\cdot\mathbf{S}_{k+1} + \mathscr{H}^n_{i,j,k-1}\cdot\mathbf{S}_k]$$

$$\mathbf{U}^{n+1}_{i,j,k} = \frac{1}{2}\left\{\mathbf{U}^n_{i,j,k} + \tilde{\mathbf{U}}^{n+1}_{i,j,k} - \frac{\Delta t}{\mathrm{vol}_{i,j,k}}[\tilde{\mathscr{H}}^{n+1}_{i,j+1,k}\cdot\mathbf{S}_{j+1} + \tilde{\mathscr{H}}^{n+1}_{i,j,k}\cdot\mathbf{S}_j + \tilde{\mathscr{H}}^{n+1}_{i+1,j,k}\cdot\mathbf{S}_{i+1} + \tilde{\mathscr{H}}^{n+1}_{i,j,k}\cdot\mathbf{S}_i + \tilde{\mathscr{H}}^{n+1}_{i,j,k+1}\cdot\mathbf{S}_{k+1} + \tilde{\mathscr{H}}^{n+1}_{i,j,k}\cdot\mathbf{S}_k]\right\} \tag{3}$$

where the subscripts i, j, and k refer to the geometrical location of the cell (see Fig. 2), and the superscripts refer to times $t = n\Delta t$ where Δt is the time step or increment that the solution is advanced during each cycle of the above two equations. The mean values $\mathbf{U}^n_{i,j,k}$ of the flow variables in the cell at time t are defined by

$$\mathbf{U}^n_{i,j,k} = \frac{\iiint_{\mathrm{vol}_{i,j,k}(t)} \mathbf{U}\, d\,\mathrm{vol}}{\iiint_{\mathrm{vol}_{i,j,k}(t)} d\,\mathrm{vol}} \tag{4}$$

where $\mathrm{vol}_{i,j,k}(t)$ is the small but finite volume of the cell at that time step and, finally, $\mathscr{H}^n_{i,j,k} = \mathscr{H}(\mathbf{U}^n_{i,j,k})$. This difference method will be used to illustrate the concept of operator splitting, although it may be applied to other numerical techniques as well.

The condition on Δt necessary for the stability of the above method is that the numerical domain of dependence must include all of the physical one. For the general case of an arbitrary nonorthogonal nonequispaced mesh composed of topological hexahedra, the necessary stability condition becomes

$$\Delta t \leqq \min_{i,j,k}\left\{\frac{\mathrm{vol}_{i,j,k}}{[|\mathbf{q}\cdot\mathbf{S}_i| + |\mathbf{q}\cdot\mathbf{S}_j| + |\mathbf{q}\cdot\mathbf{S}_k| + a(S_i^2 + S_j^2 + S_k^2)^{1/2}]_{i,j,k}}\right\} \tag{5}$$

where $a = a(\rho, p)$ is the local speed of sound. This relation, the CFL condition, must also be satisfied for convergence.

Applying the time-split, or as is sometimes called the fractional-step,[35] concept to Eq. (3) yields

$$\left.\begin{aligned}\tilde{\mathbf{U}}^{n+1/3}_{i,j,k} &= \mathbf{U}^n_{i,j,k} - \frac{\Delta t}{\mathrm{vol}_{i,j,k}}(\mathscr{H}^n_{i,j,k}\cdot\mathbf{S}_{j+1} + \mathscr{H}^n_{i,j-1,k}\cdot\mathbf{S}_j)\\ \mathbf{U}^{n+1/3}_{i,j,k} &= \frac{1}{2}\left[\mathbf{U}^n_{i,j,k} + \tilde{\mathbf{U}}^{n+1/3}_{i,j,k} - \frac{\Delta t}{\mathrm{vol}_{i,j,k}}\times(\tilde{\mathscr{H}}^{n+1/3}_{i,j+1,k}\cdot\mathbf{S}_{j+1} + \tilde{\mathscr{H}}^{n+1/3}_{i,j,k}\cdot\mathbf{S}_j)\right]\end{aligned}\right\} \tag{6a}$$

$$\left.\begin{aligned}\tilde{\mathbf{U}}^{n+2/3}_{i,j,k} &= \mathbf{U}^{n+1/3}_{i,j,k} - \frac{\Delta t}{\mathrm{vol}_{i,j,k}}(\mathscr{H}^{n+1/3}_{i,j,k}\cdot\mathbf{S}_{i+1} + \mathscr{H}^{n+1/3}_{i-1,j,k}\cdot\mathbf{S}_i)\\ U^{n+2/3}_{i,j,k} &= \frac{1}{2}\left[\mathbf{U}^{n+1/3}_{i,j,k} + \mathbf{U}^{n+2/3}_{i,j,k} - \frac{\Delta t}{\mathrm{vol}_{i,j,k}}\times(\tilde{\mathscr{H}}^{n+2/3}_{i+1,j,k}\cdot\mathbf{S}_{i+1} + \tilde{\mathscr{H}}^{n+2/3}_{i,j,k}\cdot\mathbf{S}_i)\right]\end{aligned}\right\} \tag{6b}$$

$$\left.\begin{aligned}\tilde{\mathbf{U}}^{n+1}_{i,j,k} &= \mathbf{U}^{n+2/3}_{i,j,k} - \frac{\Delta t}{\mathrm{vol}_{i,j,k}}(\mathscr{H}^{n+2/3}_{i,j,k}\cdot\mathbf{S}_{k+1} + \mathscr{H}^{n+2/3}_{i,j,k-1}\cdot\mathbf{S}_k)\\ \mathbf{U}^{n+1}_{i,j,k} &= \frac{1}{2}\left[\mathbf{U}^{n+2/3}_{i,j,k} + \tilde{\mathbf{U}}^{n+1}_{i,j,k} - \frac{\Delta t}{\mathrm{vol}_{i,j,k}}\times(\tilde{\mathscr{H}}^{n+1}_{i,j,k+1}\cdot\mathbf{S}_{k+1} + \tilde{\mathscr{H}}^{n+1}_{i,j,k}\cdot\mathbf{S}_k)\right]\end{aligned}\right\} \tag{6c}$$

This set of equations can be written more conveniently in operator notation. Let $L_x(\Delta t)$ denote the operation performed by the set of Eqs. (6a) in advancing the solution from $\mathbf{U}^n_{i,j,k}$ to $\mathbf{U}^{n+1/3}_{i,j,k}$, i.e.,

$$\mathbf{U}^{n+1/3}_{i,j,k} = L_x(\Delta t)\mathbf{U}^n_{i,j,k}$$

Let $L_y(\Delta t)$ and $L_z(\Delta t)$ be similarly defined by the next two sets, Eqs. (6b) and (6c). Stability conditions can be determined analytically for each operator. For $L_x(\Delta t)$

$$\Delta t_x \leqq \min_{i,j,k}\left\{\frac{\mathrm{vol}_{i,j,k}}{(|\mathbf{q}\cdot\mathbf{S}_j| + aS_j)_{i,j,k}}\right\} \tag{7a}$$

For $L_y(\Delta t)$

$$\Delta t_y \leqq \min_{i,j,k}\left\{\frac{\mathrm{vol}_{i,j,k}}{(|\mathbf{q}\cdot\mathbf{S}_i| + aS_i)_{i,j,k}}\right\} \tag{7b}$$

and for $L_z(\Delta t)$

$$\Delta t_z \leqq \min_{i,j,k}\left\{\frac{\mathrm{vol}_{i,j,k}}{(|\mathbf{q}\cdot\mathbf{S}_k| + aS_k)_{i,j,k}}\right\} \tag{7c}$$

These requirements, again necessary for convergence, are the one-dimensional CFL conditions. Thus, the sequence of operators

$$L_z(\Delta t)L_y(\Delta t)L_x(\Delta t)$$

representing Eqs. (6) can advance the numerical solution from $\mathbf{U}^n_{i,j,k}$ to $\mathbf{U}^{n+1}_{i,j,k}$ and is stable if

$$\Delta t \leqq \min(\Delta t_x, \Delta t_y, \Delta t_z) \tag{7d}$$

Note that this condition is always less restrictive on the maximum allowable time-step size than that of the unsplit difference scheme because the number and magnitude of positive terms summed in the denominator of Eqs. (7) are smaller than that of Eq. (5). Consequently, a larger time step is possible. Unfortunately, the sequence is only of first-order accuracy because of the noncommutativity of $L_z(\Delta t)$, $L_y(\Delta t)$, and $L_x(\Delta t)$. However, the component operators can be arranged in a symmetric sequence that can be shown to be second-order accurate. For example, if the order of the three sets of Eqs. (6) is reversed for each new n, the following symmetric sequence results:

$$L_x(\Delta t)L_y(\Delta t)L_z(\Delta t)L_z(\Delta t)L_y(\Delta t)L_x(\Delta t)$$

that can advance the solution from $\mathbf{U}^n_{i,j,k}$ to $\mathbf{U}^{n+2}_{i,j,k}$ with second-order accuracy.

Thus far the increase in the size of the allowable time step has been the only advantage gained by splitting. MacCormack and Paullay,[32] however, have pointed out another major advantage demonstrated by the following example. In many flow problems, the physical rate of propagation of information per cell is much larger in one coordinate direction than in another. For instance, if $\Delta t_y \leqq \frac{1}{2}\Delta t_z$, information can physically travel from only half as many cells in the y direction as in the z direction to influence a given point per unit of time. For this case, if either the conventional or split methods, either Eqs. (3) or (6), were used to advance the numerical solution, Δt for stability must be at most Δt_y. Consequently, the method is operating in the z direction at what amounts to half speed (at a CFL number in the z direction of at most $\frac{1}{2}$). As the calculation proceeds, the numerical method is allowing twice as much data in the z direction as are needed to influence the solution at a given cell. For this case, however, it is simple to construct a symmetric sequence of difference operators, each operating at CFL numbers near 1, to advance the solution. The sequence

$$L_x(\Delta t)L_y(\Delta t)L_z(2\Delta t)L_y(\Delta t)L_x(\Delta t)$$

where Δt is near but not larger than the value Δt_y can advance the solution from $\mathbf{U}^n_{i,j,k}$ to $\mathbf{U}^{n+2}_{i,j,k}$ with second-order accuracy. Differences in the z direction need only be calculated half as often as formerly, and the number of operators in the sequence is reduced by $\frac{1}{6}$. The computational efficiency is thereby increased. The method has adjusted so that the solution in a given cell is influenced in time by only half as many surrounding cells in the z direction as before, and the numerical and physical domains of dependence and influence are more accurately matched.

Computational Cell Network

For application of this finite-difference technique to blunt-body problems, the flowfield is divided into small topological hexahedra by a system of rays positioned in space (see Fig. 3). The partitioning is such that the innermost layer of cells lies on

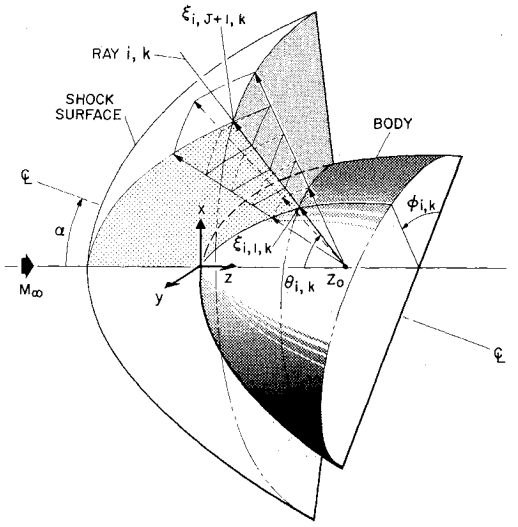

Fig. 3 Partitioning of the shock layer into topological hexahedra.

the body and the outermost in the shock layer coincides with the shock surface. The cells compose a mesh network that is floating in time and always exactly fills the time-dependent shock layer. The other boundaries are the pitch plane of symmetry and a downstream boundary immersed in supersonic flow. This mesh (Fig. 3) is quite general and permits a very wide range of body shapes to be studied. The ray i,k is specified by its two angles $\theta_{i,k}$ and $\phi_{i,k}$ made with the z and x axes and its intersection z_0 with the z axis. The distance $\xi_{i,j,k}$ along the ray between the body and the bow shock is divided into J segments. The rays are fixed in time, and the shock position on each ray is determined by integrating

$$d(\xi_{i,J+1,k}-\xi_{i,1,k})/dt = \langle W_{i,k}\rangle_{\text{av}} \tag{8}$$

where $\langle W_{i,k}\rangle_{\text{av}}$ is the simple average of the projections onto the ray i,k of the velocities of the four shock segments adjacent to the ray. As time proceeds, the cells distend and distort within pyramidal columns bounded by the fixed rays.

To further explain this mesh adjustment, a detailed view of the cell i, J, k and the four-sided segment of the shock surface mapped out by the four points $Q_{i,k}$, $Q_{i,k-1}$, $Q_{i-1,k-1}$, $Q_{i-1,k}$ that are the intersections with the four rays defining the cell edges is depicted in Fig. 4a. This shock segment is approximated by a plane so fitted that it contains the point Q_a, which is the average of the four corner points and is parallel to the two unit vectors $\hat{e}_1$ and $\hat{e}_2$ defined by the line segments $(Q_{i,k}, Q_{i-1,k-1})$ and $(Q_{i,k-1}, Q_{i-1,k})$. The unit normal vector, consequently, is determined by $\hat{\eta}_s = \hat{e}_1 \times \hat{e}_2$. This shock plane, of course, does not necessarily contain all or any of the four corner points. To integrate Eq. (8) numerically, the shock velocity λ_{η_s} normal to this plane must first be found from the Rankine-Hugoniot relations for a moving discontinuity[36]:

$$\begin{aligned} q_{\eta_s,\infty} - \lambda_{\eta_s} &= m/\rho_\infty \\ m &= [(p_2-p_\infty)/(1/\rho_\infty - 1/\rho_2)]^{1/2} \\ \varepsilon_2(p_2,\rho_2) - \varepsilon_\infty(p_\infty,\rho_\infty) &= \tfrac{1}{2}(p_2+p_\infty)(1/\rho_\infty - 1/\rho_2) \end{aligned} \tag{9}$$

where $q_{\eta_s} = \mathbf{q}\cdot\hat{\eta}_s$, and the variables with subscript 2 are the flow quantities just behind the discontinuity while those with ∞ denote freestream values. These three equations relate the velocity of the shock wave to the flow properties in surrounding cells; e.g., if p_2 is known, then λ_{η_s} can be determined from Eqs. (9).

The geometry of the actual shock displacement is displayed in Fig. 4b. The pressure p_2 at point Q_a is obtained by a quadratic extrapolation procedure using the pressures in the cells J, $J-1$, and $J-2$ within the i,k column. The shock velocity $W_{i,k}$ corresponding to λ_{η_s} but in the direction of the i,k ray is seen to be $W_{i,k} = \lambda_{\eta_s}/\cos\beta$ where β is the angle between the normal $\hat{\eta}_s$ and the i,k ray. The expression for $W_{i,k}$ derived from Eqs. (9) therefore becomes

$$W_{i,k} = (q_{\eta_s,\infty} - m/\rho_\infty)/\cos\beta \tag{10}$$

Exactly the same procedure is carried out for the other three shock segments surrounding the i,k ray, and the resulting four values of $W_{i,k}$ are then averaged to yield a single value $\langle W_{i,k}\rangle_{\text{av}}$ for the shock velocity along that fixed ray. This value enables Eq. (8) to be integrated numerically, and the new shock position $\xi_{i,J+1,k}$ can be determined for all i and k.

Initial and Boundary Conditions

Because the governing equations are hyperbolic and the subsonic region is bounded by supersonic flow, the time-dependent method is well posed as an initial-boundary-value problem. To commence the calculation, a complete initial field must be specified at all points, but it can be quite approximate since asymptotic solutions of time-dependent blunt-body problems have been observed to be virtually independent of the initial conditions.[28,30]

Specifically, our initial flowfield is built up in the following way. A shock surface, axisymmetric about the wind direction and positioned at some guessed standoff distance, is generated by a quadratic function of the latitudinal angle θ. The slope of this surface can thus be determined at any given point, and

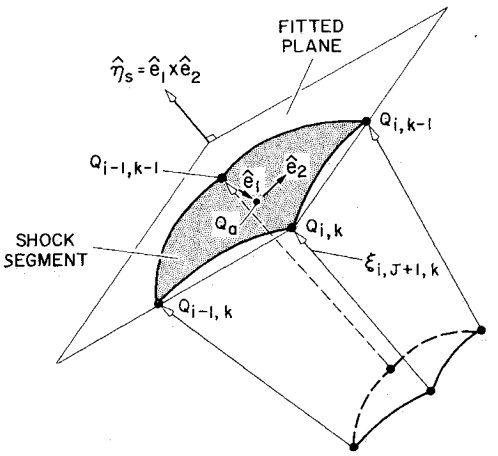

a) A typical computational cell located just behind the bow wave

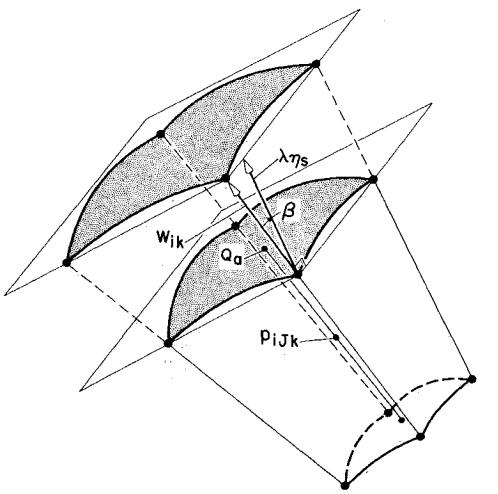

b) Shock-wave movement in time

Fig. 4 Determination of bow-wave location.

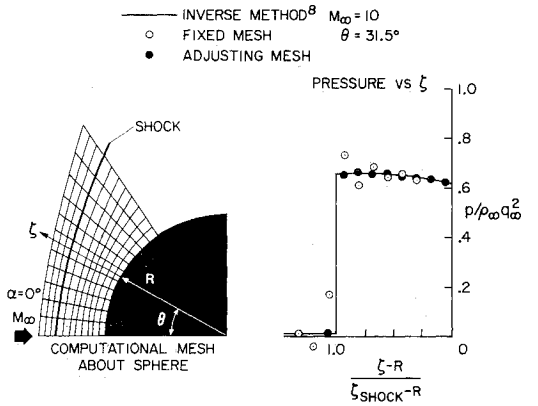

Fig. 5 The effect on pressure distribution of adjusting the mesh network to the motion of the shock wave. Three freestream cells are differenced for the fixed mesh, none for the adjusting mesh.

the flow properties there are then calculated from freestream conditions by use of the Rankine-Hugoniot shock relations. On the body, pressure is derived from a Newtonian formula, and the entropy there is set to the same value as that for a streamline passing through a normal shock. With these two properties, the density and velocity components can be found by using the equation of state and integrated steady energy relation. Finally, the flow properties within the shock layer are then specified by linearly interpolating between the shock and body values along each pyramidal column of cells.

For the inviscid calculations presented here, three distinct types of boundaries are encountered at the edges of the over-all mesh; we term them entrance, exit, and streamline boundaries. Along the entrance boundary the dependent variables **U** are held constant at their supersonic freestream values, while at the exit they are calculated using one-sided differences. Across cell faces coincident with a streamline boundary, such as an impervious body, no transport is allowed. The only variable actually needed at such a cell face is the pressure, which can be expressed in terms of the interior mesh values of pressure and the derivative of pressure normal to the face. This derivative, $\partial p/\partial \eta|_{\text{body}}$ is obtained from the momentum equation normal to a streamline:

$$\left.\frac{\partial p}{\partial \eta}\right|_{\text{body}} = \rho(u^2F_{xx}+v^2F_{yy}+w^2F_{zz}+2uvF_{xy}+2uwF_{xz}+2vwF_{yz})\times (F_x^2+F_y^2+F_z^2)^{-1/2}$$

where the body is the surface $F(x, y, z) = 0$ and the subscripts indicate partial differentiation with respect to that variable.

Importance of Mesh Adjustment

This finite-volume procedure does not necessarily require that the mesh network float in time—it can remain stationary. When the grid is permanently fixed, our numerical technique more closely resembles the way in which previous methods have captured shock waves in their solutions, but unfortunately yields solutions that contain oscillations in the properties near the discontinuity, a feature that is characteristic of this approach. We have found, however, that adjusting the mesh in time so that the cells adjacent to the shock surface are aligned with it reduces the oscillatory nature of the solution. This reduction comes about from such an alignment because the fluxes sweeping across the interface between cells located in the freestream and their neighbors in the shock layer are then exactly the components of mass, momentum, and energy normal to the shock surface. Since this method conserves the fluxes through these cells, it is performing numerically the same operation as the analytical derivation of the Rankine-Hugoniot relations from the equations of motion and thus precisely determines the flow properties across the shock wave.

Figure 5 illustrates the improvement in the solution brought about by floating the mesh. Two blunt-body solutions for flow past a sphere at $M_\infty = 10$ are shown, one using a fixed mesh and the other an adjusting one. Almost total elimination of fluctuations in the pressure distribution near the bow shock was achieved by adjusting the mesh. The final differences between the two meshes were actually quite small, on the order of the thickness of the mesh lines drawn in Fig. 5. It appears then that even the slightest misalignment of the cells can produce dramatic oscillations in the solution.

As an additional advantage, adjusting the mesh eliminates the necessity, either for accuracy or stability, of solving the flow equations in cells located upstream from the shock wave. Properties in those cells are simply set and maintained at their freestream values, thereby significantly reducing the computation and storage requirements without any accompanying loss of accuracy or convergence speed. The validity of this procedure has been established by comparisons between results calculated with and without freestream differencing and is further substantiated in the following sections for several blunt-body flows.

Discussion of Some Results

The method has been described for application to general three-dimensional flow, but can be easily specialized to plane and axisymmetric flows by specifying the appropriate shape of the computational cell. In plane flow, for example, two opposite sides of the hexahedron in Fig. 2, say the k and $k+1$ faces, are fixed parallel to each other on each and every cell, while for axisymmetric flow they are canted at some arbitrary but constant wedgelike angle. In both cases, however, flow cannot cross these k and $k+1$ faces; therefore, only one layer or plane of cells need be computed.

For several representative examples of axisymmetric and planar blunt-body flow, both calculated and experimentally measured shock shapes and density distributions are displayed and discussed. The density distribution along the stagnation streamline was deemed most appropriate because on the axis the computation cells are wedge-shaped and of smallest volume, and, consequently, the method is more susceptible to numerical difficulty and thus probably least accurate there. Such a comparison then should provide a good indication of the over-all accuracy of the entire flowfield. Flows past sphere-cones for two angles of attack are also presented and, for one case, the shock shape is compared with available wind-tunnel data.

Axisymmetric Flow Results

Figure 6 shows numerical results for a sphere located in a freestream of $M_\infty = 10$ and $\gamma = \frac{7}{5}$ compared with those calculated

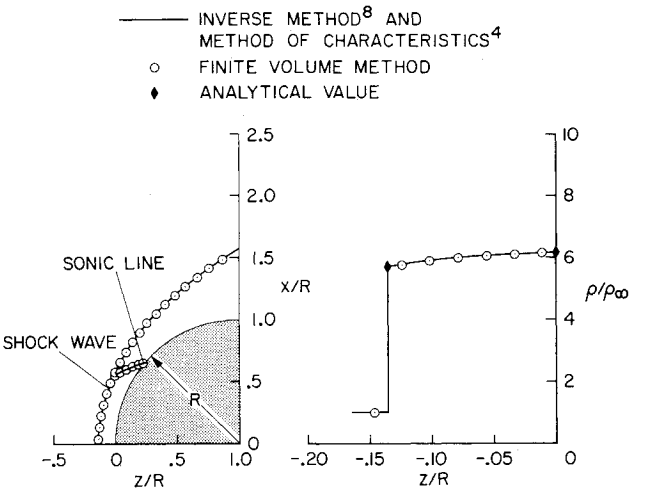

Fig. 6 Shock shape, sonic line, and stagnation-line density distribution for perfect-gas flow past a sphere at $M_\infty = 10$ and $\gamma = \frac{7}{5}$.

by the inverse method of Lomax and Inouye[8] and continued by the method of characteristics,[4] the accuracy of which has been demonstrated previously. The shock shape, sonic line, and stagnation-line density distribution are virtually identical. Our numerical computation used 6 cells across the shock layer and 19 around the body, while the inverse method employed a 10×60 grid for its corresponding field. A similar display of results at $M_\infty = 1.3$, for which the inverse method is inappropriate, is compared with the interferometer measurements of Gooderum and Wood[37] in Fig. 7. The agreement in shock shape and density variation is quite reasonable for this case, especially when the increase in cell size due to the large expanse of the subsonic region is considered. The discrepancy is at most about 5% and occurs just behind the bow wave where the interferograms are least accurate. At that location, a more relevant comparison is between the numerical results and analytical values (indicated in Fig. 7 by diamond-shaped symbols). The analytic density just behind the normal shock is obtained from the Rankine-Hugoniot relations, and the corresponding density on the body is then found from this value by use of the isentropic flow relations. As shown in Fig. 7, the numerical calulations agree well with the analytical values. Of particular importance is the smoothness of the density variation near the rear of the shock. Figures 6 and 7 clearly illustrate the ability of this method at both high and low Mach numbers to accurately approximate weak solutions of Eq. (1) without the usually large fluctuations in downstream flow properties and without the need to difference the freestream flow.

Plane-Flow Results

Figures 8 and 9 show numerical calculations for a circular cylinder located in a stream at Mach numbers of 4 and 1.8 for $\gamma = \frac{7}{5}$. At $M_\infty = 4$ (Fig. 8), excellent correlation is obtained with the calculations by Belotserkovskii[38] and the combined inverse and characteristic method, although all computed shock shapes uniformly begin to differ slightly in the highly supersonic region from the experimental one measured by Kim.[39] For $M_\infty = 1.8$ (Fig. 9), considerable differences between numerical and experimental values begin to occur about four body radii from the origin where the computational cells are largest. The measured shock position tends to be upstream of the calculated one,

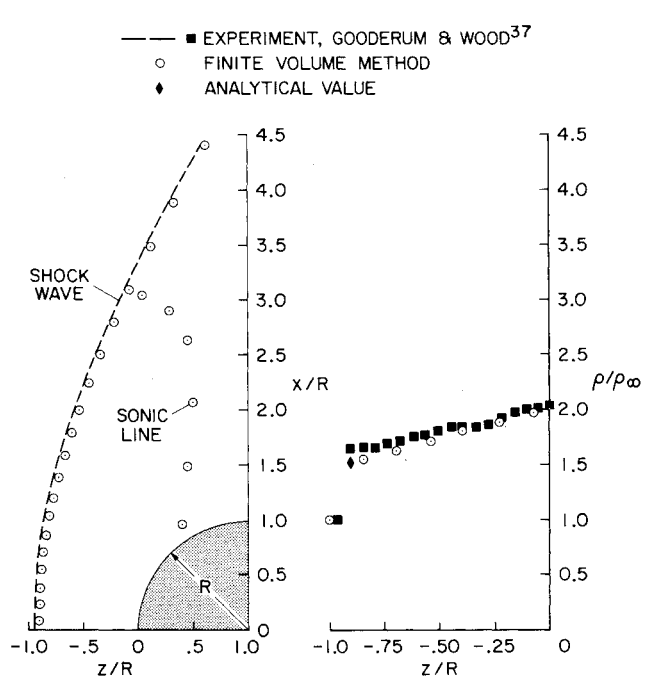

Fig. 7 Shock shape and density distribution along the axis for perfect-gas flow past a sphere at $M_\infty = 1.3$ and $\gamma = \frac{7}{5}$.

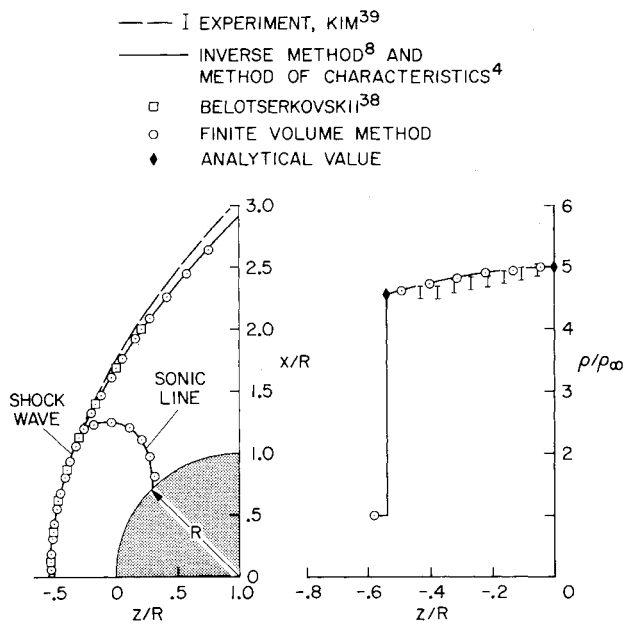

Fig. 8 Shock shape, sonic line, and stagnation-line density distribution for perfect-gas flow past a circular cylinder at $M_\infty = 4$ and $\gamma = \frac{7}{5}$.

similar to the trend of the discrepancy indicated in Fig. 8. Part of this disagreement could conceivably be due to experimental errors or viscous effects. For both cases, however, the density variation along the stagnation streamline compares very favorably with both the experimental data and the numerical calculations of other methods.

Three-Dimensional Results

For flow past sphere-cone bodies at angle of attack, the flowfield was divided into 15 cells around the body in the latitudinal direction, 9 in the meridional, and 6 across the shock layer. The z-axis is aligned with the wind direction and the xz plane lies in the pitch plane of symmetry. Figure 10 presents results in the pitch plane for a sphere-cone body of 15° half-angle at 30° angle of attack in a stream for which $M_\infty = 14.9$ and $\gamma = \frac{5}{3}$. The calculated shock shape is in excellent agreement with that measured by Cleary and Duller,[40] always lying within the indicated error band associated with transcribing the shock shape from a small-scale shadowgraph to the large scale in Fig. 10. On the windward side, the sonic line touches the body near the

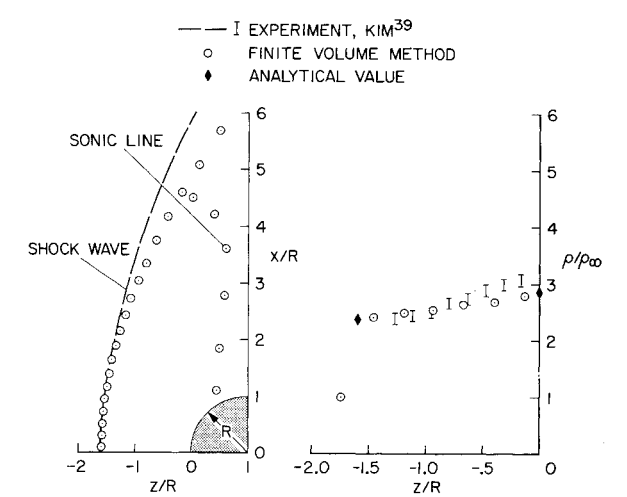

Fig. 9 Shock shape and density distribution along the axis for perfect-gas flow past a circular cylinder at $M_\infty = 1.8$ and $\gamma = \frac{7}{5}$.

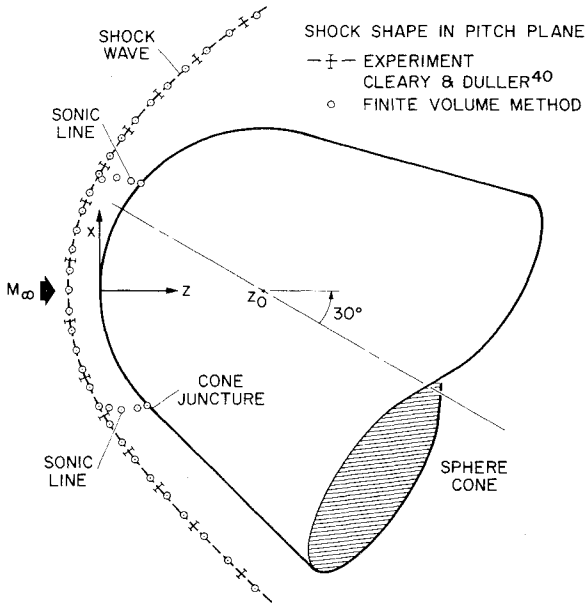

Fig. 10 Shock shape in the symmetry plane for perfect-gas flow past a sphere-cone body of 15° half-angle at $M_\infty = 14.9$, $\gamma = \frac{5}{3}$, and 30° angle of attack.

juncture point of the sphere and cone, thus showing that a part of the cone influences the region of subsonic flow.

The computed shock shape and sonic line in the pitch plane as well as perspective and cross-sectional views of the full three-dimensional shock shape of a sphere-cone of 23° half-angle immersed in a stream at $M_\infty = 10$ and $\gamma = \frac{7}{5}$ at 35° angle of attack are shown in Fig. 11. On the windward side in the pitch plane, the sonic line now stretches far downstream on the cone section of the body and differs totally in shape from that on the leeward part of the sphere. The flow is highly asymmetric, as shown in Fig. 12 from the variation of pressure distribution on the body surface. Displayed here is a contour of pressure vs latitudinal angle θ and meridional angle ϕ, where $\phi > 90°$ indicates the windward side and $\phi < 90°$ the leeward. For each value of ϕ, the pressure with increasing θ falls monotonically from its stagnation value as the flow expands around the spherical portion of the body. However, when the flow reaches the sphere-cone juncture on the windward side, it encounters an abrupt change of curvature and begins to recompress as θ increases further. For the $\phi = 170°$ line, the expansion begins to cease at about $\theta = 32°$, the sphere-cone juncture, and then recompresses monotonically to a maximum at $\theta = 68°$, after which the flow begins to expand again. This recompression starting at the juncture on the body causes a compression wave to propagate out into the flowfield, ultimately coalescing with and strengthening the bow wave, causing it to straighten with respect to the oncoming stream. This change of curvature, or inflection point, of the shock wave is clearly seen in the computed shape displayed in Fig. 11. Finally, Fig. 13 shows the calculated local-Mach-number distribution on the body surface, drawn in a manner similar to the pressure. This plot does not show $M = 0$ because the stagnation point is located in the symmetry plane that lies 10° away from our nearest data plane. It is important, however, to point out that at all exit boundaries the flow is supersonic.

Conclusions

A finite-volume method has been shown to be an accurate, easily-programmed procedure for calculating blunt-body flow at low supersonic Mach numbers as well as relatively large angles of attack. Shock waves are automatically determined as part of the solution, and adjusting the mesh in time to the shock surface yields very sharp jumps in the flow properties across the shock.

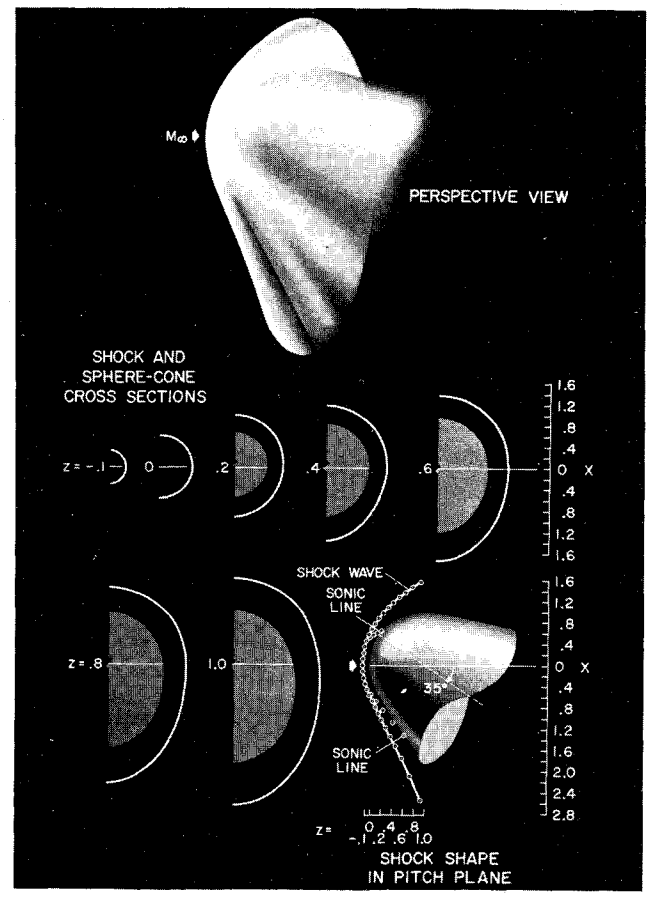

Fig. 11 Shock shape in full perspective, cross-sectional, and pitch-plane views for a sphere-cone body of 23° half-angle in a perfect gas at $M_\infty = 10$, $\gamma = \frac{7}{5}$, and 35° angle of attack.

This way of handling discontinuities poses neither difficulties nor instabilities as the oncoming Mach number decreases and the bow wave weakens to a Mach wave, and allows very low Mach-number flows to be computed. Time splitting has been incorporated into the difference method to increase the size of the allowable time increment and thus increase the convergence rate, as well as the numerical efficiency. Several refinements can be

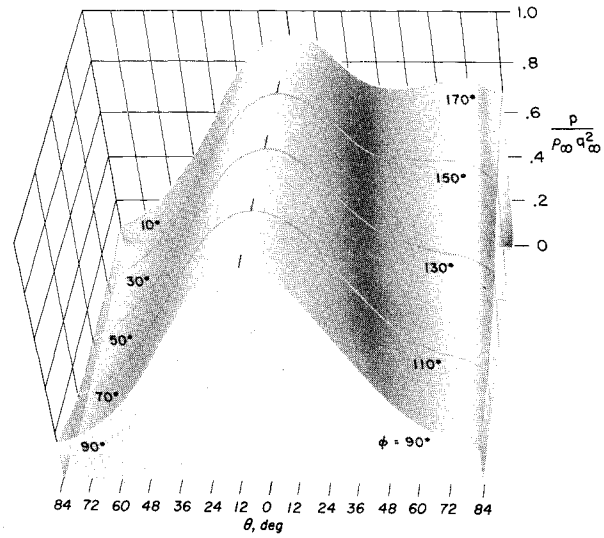

Fig. 12 Computed pressure distribution on the body surface for the flow in Fig. 11.

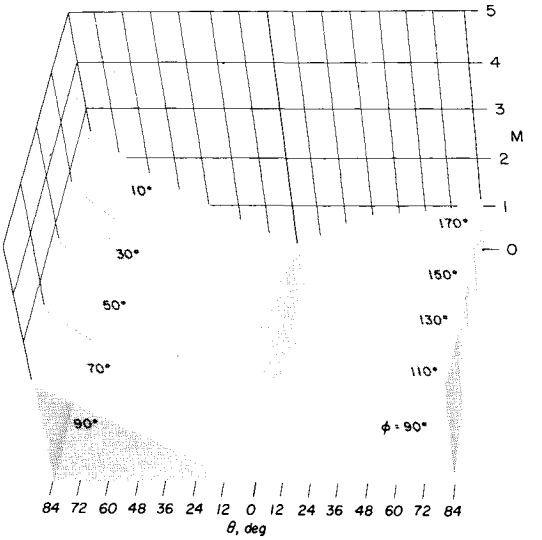

Fig. 13 Computed Mach number on the body surface for the flow in Fig. 11.

incorporated simply. For instance, real-gas effects enter only through the equation of state that is easily exchanged in the algorithm, and the mesh can be further generalized so that, instead of the cell rays emanating from only one point, they can be made to originate at any number of points arbitrarily located in space.

References

[1] Kutler, P., Reinhardt, W. A., and Warming, R. F., "Multishocked, Three-Dimensional Supersonic Flowfields with Real Gas Effects," *AIAA Journal*, Vol. 11, No. 5, May 1973, pp. 657–664.

[2] Thomas, P. D., Vinokur, M., Bastianon, R. A., and Conti, R. J., "Numerical Solution for Three-Dimensional Inviscid Supersonic Flow," *AIAA Journal*, Vol. 10, No. 7, July 1972, pp. 887–894.

[3] Moretti, G., Grossman, B., and Marconi, F., Jr., "A Complete Numerical Technique for the Calculation of Three-Dimensional Inviscid Supersonic Flows," AIAA Paper 72-192, San Diego, Calif., 1972.

[4] Inouye, M., Rakich, J. V., and Lomax, H., "A Description of Numerical Methods and Computer Programs for Two-Dimensional and Axisymmetric Supersonic Flow Over Blunt-Nosed and Flared Bodies," TN D-2970, 1965, NASA.

[5] Rakich, J. V., "Three-Dimensional Flow Calculations by the Method of Characteristics," *AIAA Journal*, Vol. 5, No. 10, Oct. 1967, pp. 1906–1908.

[6] Hayes, W. D. and Probstein, R. F., *Hypersonic Flow Theory*, 2nd ed., Academic Press, New York, 1966.

[7] Van Dyke, M., "The Supersonic Blunt-Body Problem—Review and Extension," *Journal of Aerospace Sciences*, Vol. 25, 1958, pp. 485–496.

[8] Lomax, H. and Inouye, M., "Numerical Analysis of Flow Properties About Blunt Bodies Moving at Supersonic Speeds in an Equilibrium Gas," TR R-204, 1964, NASA.

[9] Webb, H. G., Jr., Dressler, H. S., Adler, B. K., and Waiter, S. A., "Inverse Solution of Blunt-Body Flowfields at Large Angle of Attack," *AIAA Journal*, Vol. 5, No. 6, June 1967, pp. 1079–1085.

[10] Dorodnitsyn, A. A., "A Contribution to the Solution of Mixed Problems of Transonic Aerodynamics," *Advances in Aeronautical Sciences*, Vol. 2, Pergamon Press, New York, 1959, pp. 832–843.

[11] Belotserkovskii, O. M. and Chushkin, P. I., "The Numerical Solution of Problems in Gas Dynamics," *Basic Developments in Fluid Dynamics*, Vol. 1, edited by M. Holt, Academic Press, New York, 1965, pp. 1–126.

[12] Telenin, G. F. and Tinyakov, G. P., "A Method of Calculating the Three-Dimensional Flow Past a Body with an Attached Shock Wave," *Soviet Physics Doklady*, English Translation, Vol. 9, 1964, pp. 132–133.

[13] MacCormack, R. W. and Warming, R. F., "Survey of Computational Methods for Three-Dimensional Supersonic Inviscid Flows with Shocks," *Advances in Numerical Fluid Dynamics*, AGARD Lecture Series 64, Brussels, Belgium, Feb. 1973.

[14] Bohachevsky, I. O. and Mates, R. E., "A Direct Method for Calculation of Flow About an Axisymmetric Blunt Body at Angle of Attack," *AIAA Journal*, Vol. 4, No. 5, May 1966, pp. 776–782.

[15] Moretti, G. and Abbett, M., "A Time Dependent Computational Method for Blunt Body Flows," *AIAA Journal*, Vol. 4, No. 12, Dec. 1966, pp. 2136–2141.

[16] Evans, M. W. and Harlow, F. H., "The Particle-in-Cell Method for Hydrodynamic Calculations," Rept. LA-2139, 1957, Los Alamos Scientific Lab., Los Alamos, N. Mex.

[17] Harlow, F. H., "The Particle-in-Cell Computing Method for Fluid Dynamics," *Methods in Computational Physics*, Vol. 3, edited by B. Alder, S. Fernbach, and M. Rotenberg, Academic Press, New York, 1964, pp. 319–343.

[18] Bohachevsky, I. O. and Rubin, E. L., "A Direct Method for Computation of Nonequilibrium Flows with Detached Shock Waves," *AIAA Journal*, Vol. 4, No. 4, April 1966, pp. 600–607.

[19] Gentry, R. A., Martin, R., and Daly, B. J., "An Eulerian Differencing Method for Unsteady Compressible Flow Problems," *Journal of Computational Physics*, Vol. 1, 1966, pp. 87–118.

[20] Barnwell, R. W., "Numerical Results for the Diffraction of a Normal Shock Wave by a Sphere and for the Subsequent Transient Flow," TR R-268, 1967, NASA.

[21] Godunov, S. K., Zabrodin, A. V., and Prokopov, G. P., "A Computational Scheme for Two-Dimensional Nonstationary Problems of Gas Dynamics and Calculation of the Flow from a Shock Wave Approach a Stationary State," *USSR Computational Mathematics and Mathematical Physics*, English Translation, 1961, pp. 1187–1219.

[22] Masson, B. S., Taylor, T. D., and Foster, R. M., "Application of Godunov's Method to Blunt-Body Calculations," *AIAA Journal*, Vol. 7, No. 4, April 1969, pp. 694–698.

[23] McNamara, W., "FLAME Computer Code for the Axisymmetric Interaction of a Blast Wave with a Shock Layer in a Blunt Body," *Journal of Spacecraft and Rockets*, Vol. 4, No. 6, June 1967, pp. 790–795.

[24] Rusanov, V. V., "Three-Dimensional Flow About an Arbitrary Blunt Body," *Aerospace Proceedings*, Vol. 1, edited by J. Bradbrooke, J. Bruce, and R. R. Dexter, Macmillan, 1966, pp. 291–301.

[25] Lax, P. D., "Weak Solutions of Nonlinear Hyperbolic Equations and Their Numerical Computation," *Communications on Pure and Applied Mathematics*, Vol. 7, 1954, pp. 159–193.

[26] Lax, P. D. and Wendroff, B., "System of Conservation Laws," *Communications on Pure and Applied Mathematics*, Vol. 13, 1960, pp. 217–237.

[27] Burstein, S. Z., "Finite-Difference Calculations for Hydrodynamic Flows Containing Discontinuities," *Journal of Computational Physics*, Vol. 1, 1966, pp. 198–222.

[28] Moretti, G. and Bleich, G., "Three-Dimensional Flow around Blunt Bodies," *AIAA Journal*, Vol. 5, No. 10, Oct. 1967, pp. 1557–1562.

[29] Barnwell, R. W., "A Time-Dependent Method for Calculating Supersonic Blunt-Body Flow Fields with Sharp Corners and Embedded Shock Waves," TN D-6031, 1970, NASA.

[30] Barnwell, R. W., "A Time-Dependent Method for Calculating Supersonic Angle-of-Attack Flow About Axisymmetric Blunt Bodies with Sharp Shoulders and Smooth Nonaxisymmetric Blunt Bodies," TN D-6283, 1971, NASA.

[31] Li, C. P., "Time-Dependent Solutions of Nonequilibrium Airflow Past a Blunt Body," *Journal of Spacecraft and Rockets*, Vol. 9, No. 8, Aug. 1972, pp. 571–572.

[32] MacCormack, R. W. and Paullay, A. J., "Computational Efficiency Achieved by Time Splitting of Finite Difference Operators," AIAA Paper 72-154, San Diego, Calif., 1972.

[33] Vinokur, M., "Conservation Equations of Gasdynamics in Curvilinear Coordinate Systems," *Journal of Computational Physics*, 1973, to be published.

[34] MacCormack, R. W., "Numerical Solution of the Interaction of a Shock Wave with a Laminar Boundary Layer," *Lecture Notes in Physics*, Vol. 8, Springer-Verlag, 1971, pp. 151–163.

[35] Yanenko, N. N., *The Method of Fractional Steps*, Springer-Verlag, New York, 1971.

[36] Landau, L. D. and Lifshitz, E. M., *Fluid Mechanics*, Pergamon Press, London, 1959.

[37] Gooderum, P. B. and Wood, G. P., "Density Fields Around a Sphere at Mach Numbers 1.30 and 1.62," TN 2173, 1950, NACA.

[38] Belotserkovskii, O. M., "Flow Past a Circular Cylinder with a Detached Shock," *Vychislitel'noi Matematiki*, No. 3, 1958, pp. 149–185.

[39] Kim, C. S., "Experimental Studies of Supersonic Flow Past a Circular Cylinder," *Journal of the Physical Society of Japan*, Vol. 11, 1956, pp. 439–445.

[40] Cleary, J. W. and Duller, C. E., "Effects of Angle of Attack and Bluntness on the Hypersonic Flow over a 15° Semiapex Cone in Helium," TN D-5903, 1970, NASA.